ADVANCES IN ATMOSPHERIC SCIENCES, VOL. 34, DECEMBER 2017, 1404–1414

• **Original Paper** •

Effects of Wind Fences on the Wind Environment around Jang Bogo Antarctic Research Station

Jang-Woon WANG[1], Jae-Jin KIM*[1], Wonsik CHOI[1], Da-Som MUN[1], Jung-Eun KANG[1], Hataek KWON[2], Jin-Soo KIM[3], and Kyung-Soo HAN[3]

[1]*Department of Environmental Atmospheric Sciences, Pukyong National University* 45, *Yongso-ro, Nam-gu, Busan,* 48513, *Republic of Korea*

[2]*Korea Polar Research Institute* 26, *Songdomirae-ro, Yeonsu-gu, Incheon,* 21990, *Republic of Korea*

[3]*Department of Spatial Information Engineering, Pukyong National University* 45, *Yongso-ro, Nam-gu, Busan,* 48513, *Republic of Korea*

(Received 29 December 2016; revised 22 May 2017; accepted 2 June 2017)

ABSTRACT

This study investigated the flow characteristics altered by Jang Bogo Antarctic Research Station using computational fluid dynamics (CFD) modeling. The topography and buildings around Jang Bogo Station were constructed with computer-aided-design data in the CFD model domain. We simulated 16 cases with different inflow directions, and compared the flow characteristics with and without Jang Bogo Station for each inflow direction. The wind data recorded by the site's automatic weather station (AWS) were used for comparison. Wind rose analysis showed that the wind speed and direction after the construction of Jang Bogo Station were quite different from those before construction. We also investigated how virtual wind fences would modify the flow patterns, changing the distance of the fence from the station as well as the porosity of the fence. For westerly inflows, when the AWS was downwind of Jang Bogo Station, the decrease in wind speed was maximized (−81% for west-northwesterly). The wind speed reduction was also greater as the distance of the fence was closer to Jang Bogo Station. With the same distance, the fence with medium porosity (25%–33%) maximized the wind speed reduction. These results suggest that the location and material of the wind fence should be selected carefully, or AWS data should be interpreted cautiously, for particular prevailing wind directions.

Key words: Jang Bogo Antarctic Research Station, CFD model, observation environment, wind fence, porosity

Citation: Wang, J.-W., and Coauthors, 2018: Effects of wind fences on the wind environment around Jang Bogo Antarctic Research Station. *Adv. Atmos. Sci.*, **34**(12), 1404–1414, https://doi.org/10.1007/s00376-017-6333-x.

1. Introduction

Jang Bogo Antarctic Research Station (hereafter, JB Station) is located near Terra Nova Bay, Northern Victoria Land, Antarctica. Low-pressure systems are common in this region due to the influences of the Ross Sea and Transantarctic Mountains. At JB Station, westerly winds dominate, and daily mean wind speeds range from 0.5 m s^{-1} to 38.6 m s^{-1}. Because the station is located at the bottom of a mountain slope, strong winds sweeping down the slope (i.e., katabatic winds) are common (Ma, 1992; Nylen et al., 2004; Yu et al., 2007). The maximum wind speed recorded at Terra Nova Bay is 45 m s^{-1} (Bromwich, 1989), and similarly strong winds could pose a risk to researchers at the station. A survey of visitors to the Antarctic King Sejong Station revealed that one of the most threatening elements at the station was the rapid change in wind speed and direction (Weber et al., 2016). Therefore, it is necessary to establish a plan to protect residents from wind and ensure a secure living environment at the station.

By reducing wind speed, windbreaks (i.e., wind fences) are effective at reducing the risks caused by strong winds. Most studies on the efficacy of windbreaks have been performed using wind tunnel experiments (Judd et al., 1996; Lee and Kim, 1999; You and Kim, 2009), and have shown that wind speed reductions depend primarily on the shape and porosity of the windbreak (Dong et al., 2007). In addition, Zhang et al. (2010) and Cheng et al. (2016) demonstrated that windbreaks can reduce dust-scattering by weakening near-surface wind speeds. Cheng et al. (2016) reported that windproof walls could reduce wind speeds by up to 80% in the downwind region. However, most studies have focused on the effects of wind fences installed on flat surfaces, and there are few studies concerning wind fences constructed on inclined planes, such as mountain slopes.

* Corresponding author: Jae-Jin KIM
Email: jjkim@pknu.ac.kr

Computational fluid dynamics (CFD) modeling is a useful tool for evaluating the effects of windbreaks on wind speeds in relatively small areas, such as at JB Station. Several recent studies have evaluated the observation environments around weather stations using CFD models (e.g., Tominaga et al., 2004; Stathopoulos, 2006).

In the present study, we selected a 1-km^2 area around JB Station as the model domain to quantify the effects of the construction of JB Station on the area around the site's automatic weather system (AWS) by comparing data collected before and after the construction of JB Station. In addition, we performed numerical experiments to investigate the effects on wind behavior of installing wind fences around JB Station, and assessed the effects of various wind fence porosities and distances from the station. The goal of this study was to determine the optimal porosity and location of the wind fence to reduce wind speeds around JB Station, while minimally impacting wind patterns around the AWS.

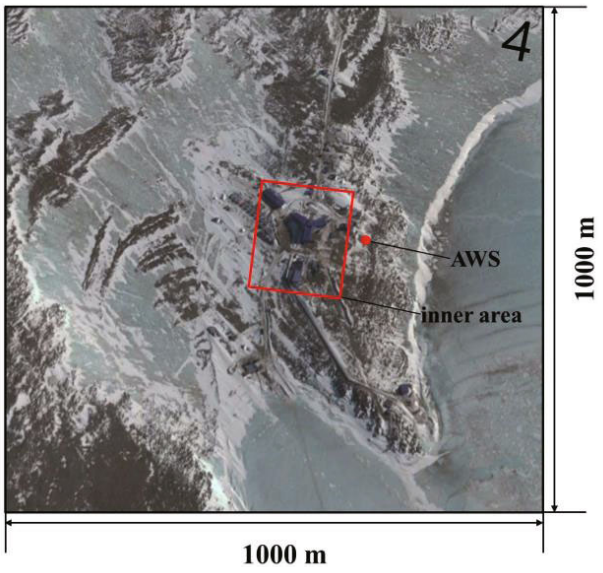

Fig. 1. Satellite image of the area around JB Station (from Google Earth, www.earth.google.com).

2. Methods

2.1. *Numerical model*

We used the same CFD model in this study as that described in Kim and Baik (2010) — a model that has been extensively validated against wind-tunnel measurement results (Kim, 2007; Kim and Baik, 2010). The model considers a three-dimensional, non-hydrostatic, non-rotating, and incompressible airflow. For the turbulence parameterization, it uses the k–ε turbulence closure scheme based on renormalization group (RNG) theory. Reynolds-averaged Navier–Stokes equations are solved numerically in a staggered grid system using the Semi-Implicit Method for the Pressure-Linked Equation algorithm and finite volume method. To consider the turbulence effects near solid wall boundaries, the model uses wall functions for the momentum, turbulence kinetic energy (TKE), and TKE dissipation rate equations suggested by Versteeg and Malalasekera (1995).

2.2. *Experimental setup*

We used a 1-km^2 area around JB Station near Terra Nova Bay, Northern Victoria Land, Antarctica (74°37.4′S, 164°13.7′E) as the target area (Fig. 1). The sea is located to the south and east of the station, and 500–700-m high mountains are to the north and west of the station. JB Station was constructed on a slope facing the sea. The red dot in Fig. 1 indicates the location of the AWS to the east of JB Station. The main building, with a height of 15 m, is the tallest building at the station.

The grid system is similar to the Arakawa C-grid system; except, at the boundaries of the numerical domain, each velocity component (U, V, W) is defined at the center of each face of a control volume, and scalar quantities such as TKE and its dissipation rate are defined at the center of the control volume. At the boundaries, both the velocity components and scalar quantities are defined at the boundary edges of the grid cells. For details about the grid system and numerical method, see Baik et al. (2003). The model used numerical domain sizes of 1000 m, 1000 m and 250 m for the x-, y- and z-axes, respectively. A uniform grid system was used and the grid intervals for the x-, y- and z-axes were 5 m, 5 m and 2.5 m, respectively. The grid intervals used in this study were relatively coarse compared to those in simulating flows for a single street canyon and/or a single obstacle. Given the much larger numerical domain for this application, we needed to use larger grid sizes due to the limitation of computation. Many previous studies focusing on neighborhood-scale flows in urban areas (horizontal domain size of ~ 1 km) have used similar or larger grid sizes (~ 10 m) (Baik et al., 2009; Gousseau et al., 2011; Gowardhan et al., 2011; Hertwig et al., 2012). Thus, the grid intervals in this study were regarded as optimal for resolving both the surrounding mountainous topography and the buildings at JB station.

Using the building construction algorithm suggested in Baik et al. (2009), and geographic information system tools, we constructed three-dimensional configurations representative of the surface boundary conditions before and after the construction of JB Station (hereafter referred to as JB-before and JB-after cases, respectively) for the CFD model (Figs. 2a and b). Referring to the Cost Action 732 guideline that the horizontal resolution in street canyons should be $\leqslant$ 2 m and the vertical domain size should be larger than six times the building height (Eichhorn, 2004), we conducted additional simulations for an idealized street canyon to determine the grid-interval dependency. The results indicated little difference with grid interval (not shown).

To investigate the effects of the construction of JB Station on the surface wind environment, numerical simulations were performed for 16 inflow directions (northerly to north-northwesterly at intervals of 22.5°) for both the JB-before and JB-after cases. In addition, we examined the effects of installing wind fences to the north and west of JB Station

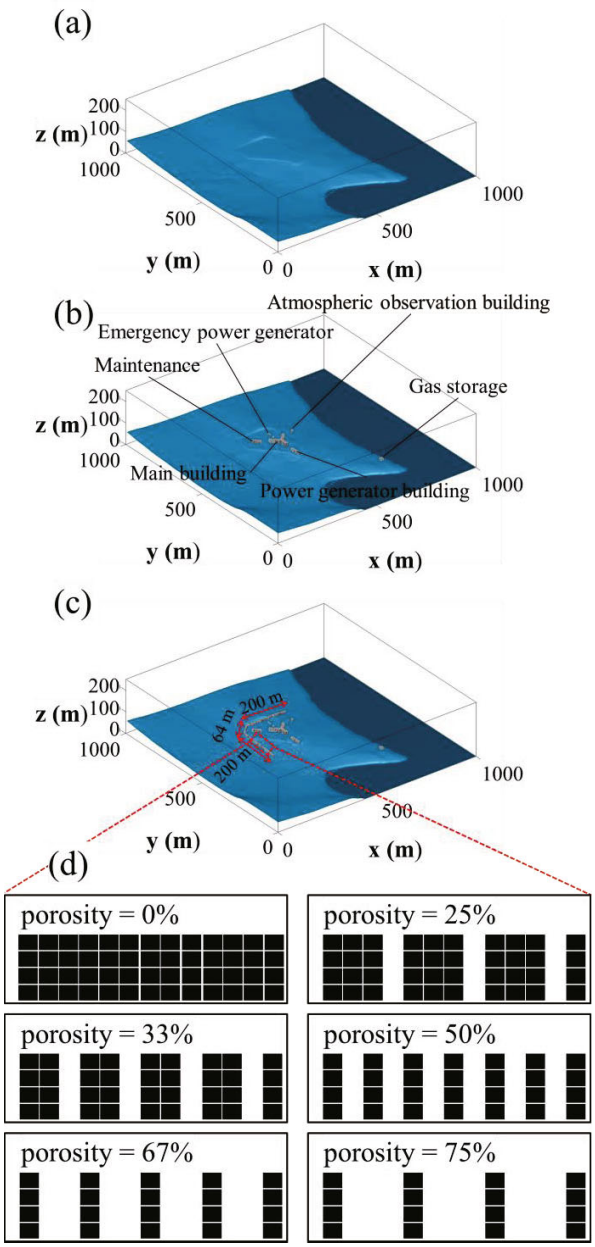

Fig. 2. Computational configurations (a) before and (b) after the construction of JB Station, and (c) after the construction of wind fences. Boxes in (d) indicate the wind-fence shapes with different porosities considered in this study.

(Fig. 2c). Wind fences with porosities of 0%, 25%, 33%, 50%, 67% and 75%, and distances from the nearest building of 2H, 4H, 6H and 8H (where the wind fence height, H, was 10 m) were considered. Wind fences were explicitly reproduced by heaping up the fences, as in constructing buildings and topography. We assumed that wind fences were vertical-pole in type because this made it easy to allocate porosity systematically (Fig. 2c). We acknowledge that assumed wind-fence shapes are idealized and that there is numerical limitation involved in not taking the real wind-fence shapes into account in the CFD model. To address this issue, we are currently developing a method that implicitly represents the wind-fence effects by adding additional drag terms to the governing equation set.

The wind-fence analysis was performed assuming westerly inflows, based on the predominance of strong katabatic winds at the station. The lengths of the wind fences to the west and north were each 200 m and the length of the wind fence connecting the two wind fences was 64 m. To obtain results sufficiently adjusted by external forcing (e.g., topography and buildings), we integrated the CFD model up to 3600 s with 0.5-s intervals. In our experience, this configuration is satisfactory in neighborhood-scale simulations.

Based on observations at the Antarctic (Mitsuhashi, 1982), we assumed log profiles at the inflow boundaries. Also, to consider winds blowing from the mountain slopes, the vertical profiles of the inflows were described as follows:

$$U(z) = \frac{u_*}{\kappa}\ln\left(\frac{z}{z_0}\right)\cos\theta\,; \tag{1}$$

$$V(z) = \frac{u_*}{\kappa}\ln\left(\frac{z}{z_0}\right)\sin\theta\,; \tag{2}$$

$$W(z) = \frac{u_*}{\kappa}\ln\left(\frac{z}{z_0}\right)\tan\alpha\,; \tag{3}$$

where u_*, κ, z_0, θ and α denote friction velocity, the von Kármán constant (0.4), roughness length (0.05), wind direction, and mountain slope (−6°), respectively. For the TKE and TKE dissipation rates, we used the vertical profiles suggested in Castro and Apsley (1997):

$$k(z) = \frac{u_*^2}{C_\mu^{1/2}}\left(1-\frac{z}{\delta}\right)^2\,; \tag{4}$$

$$\varepsilon(z) = \frac{C_\mu^{3/4}k^{3/2}}{\kappa z}\,. \tag{5}$$

Here, δ is the boundary layer depth (1000 m) and C_μ is the empirical constant for the RNG $\kappa-\varepsilon$ turbulence closure scheme (0.0845) (Yakhot et al., 1992). Zero gradient conditions are applied at the outflow boundaries. At the solid wall boundaries, the same boundary conditions as those in Kim and Baik (2010) are applied.

3. Results and discussion

3.1. *Analysis of observed surface winds*

We examined the hourly average wind data from the AWS near JB Station over about four years (8 February 2010 to 15 February 2015), excluding the period when JB Station was under construction (1 November 2011 to 31 December 2012). To investigate the effects of the presence of JB Station on the AWS observations, we analyzed wind roses for JB-before (8 February 2010 to 31 October 2012) and JB-after (1 January 2013 to 15 February 2015) cases (Fig. 3). The main wind direction differed minimally between the JB-before

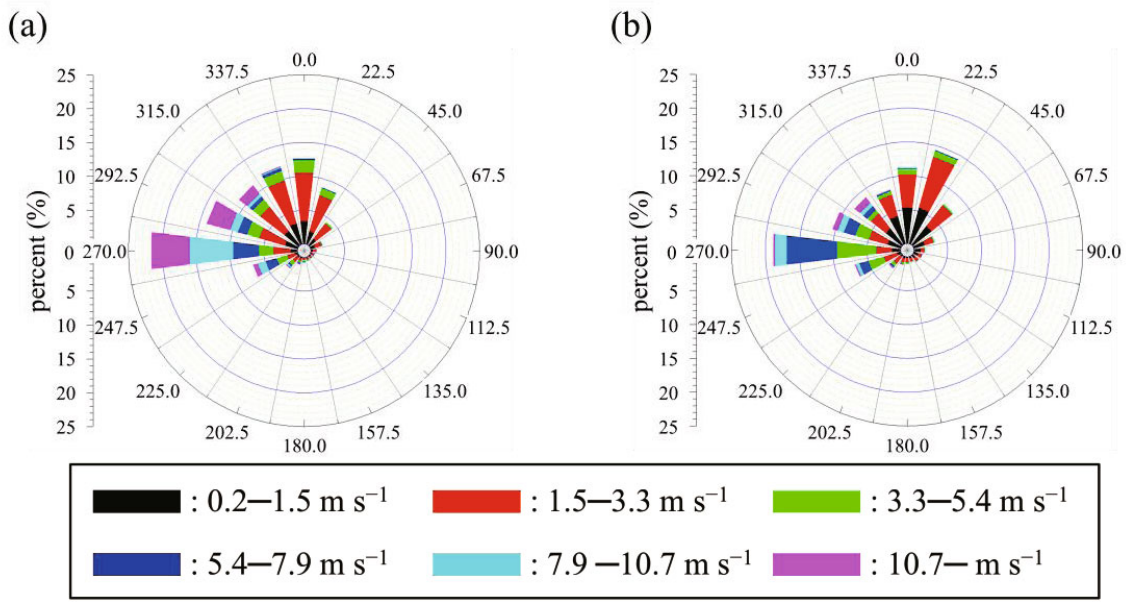

Fig. 3. Wind roses (a) before and (b) after the construction of JB Station.

and JB-after cases. The occurrence frequencies of westerly, west-northwesterly, northerly, and north-northwesterly inflows in the JB-before cases were 21.7%, 13.9%, 12.7% and 12.0%, respectively. In the JB-after cases, westerly (18.9%), north-northeasterly (14.4%), northerly (11.2%), and west-northwesterly (10.4%) flows were the most prevalent wind directions at the AWS. After the construction of JB Station, the annual mean wind speed decreased by ~ 1.5 m s^{-1} (4.7 m s^{-1} to 3.2 m s^{-1}), while wind speed in summer (December, January and February) and winter (June, July and August) decreased by 1.4 m s^{-1} (4.6 m s^{-1} to 3.2 m s^{-1}) and 2.1 m s^{-1} (5.1 m s^{-1} to 3.0 m s^{-1}), respectively.

Figure 4 shows the annual mean wind speed for each wind direction in the JB-before and JB-after cases. Westerly flows were the strongest among the 16 wind directions, decreasing by ~ 35% (8.1 m s^{-1} to 5.3 m s^{-1}) in the JB-after case. West-northwesterly and west-southwesterly flows were relatively strong, and decreased by ~ 35% (6.9 m s^{-1} to 4.5 m s^{-1}) and 27% (6.0 m s^{-1} to 4.4 m s^{-1}), respectively, in the JB-after case. Easterly flows had a mean wind speed of ~ 2.0 m s^{-1}. Relatively strong winds were predominantly westerly, due to the strong katabatic winds from the cold slope of the mountain to the west. The maximum observed wind speed was 35.9 m s^{-1} in a northwesterly direction. The hourly average wind speed analysis identified 136 extremely strong wind events ($\geqslant$ 20 m s^{-1}), which were mainly westerly. Even considering climatological variations in wind speed in Antarctica, the analysis of the wind data from the AWS revealed that the construction of JB Station markedly affected the surrounding wind environment, and induced a meaningful decrease in near-surface wind speeds. Therefore, the AWS should be moved to a more suitable location to observe surface winds and maintain the climatological continuity of data unaffected by artificial changes to the geographical features around JB Station.

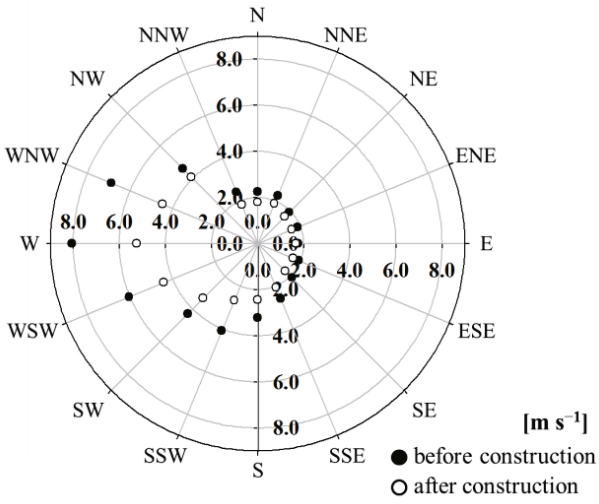

Fig. 4. Wind speeds observed at the AWS before and after the construction of JB Station.

3.2. *Analysis of the flow characteristics in the JB-before and JB-after cases*

To analyze the flow changes induced by the construction of JB Station, numerical simulations were performed for the 16 inflow directions in the JB-before and JB-after cases. In addition, detailed flow characteristics were described for the three inflow directions (westerly, north-northeasterly, and northerly) with strong katabatic winds and relatively high frequency occurrences in the wind rose analysis.

3.2.1. *Wind speed changes at the surface at the station and at the height of the AWS*

We analyzed the effects of the construction of JB Station on near-surface (z = 1.25 m) airflow at the station and wind speed and direction at the AWS (z = 5 m). Several changes

in wind speed were observed at the AWS after the construction of the station (Fig. 5a). Of the westerly winds, westerly, west-southwesterly, west-northwesterly and northwesterly wind speeds at the AWS markedly decreased. The maximum decrease (81.4%) was simulated in the west-southwesterly flow. Conversely, easterly wind speeds changed minimally, with a maximum decrease of 7.2% in the easterly flow. This was likely because the AWS is located east of JB Station, and is downwind of the station only for westerly inflows (not shown). These results are consistent with observations (Fig. 4) at JB Station (JB-before and JB-after cases).

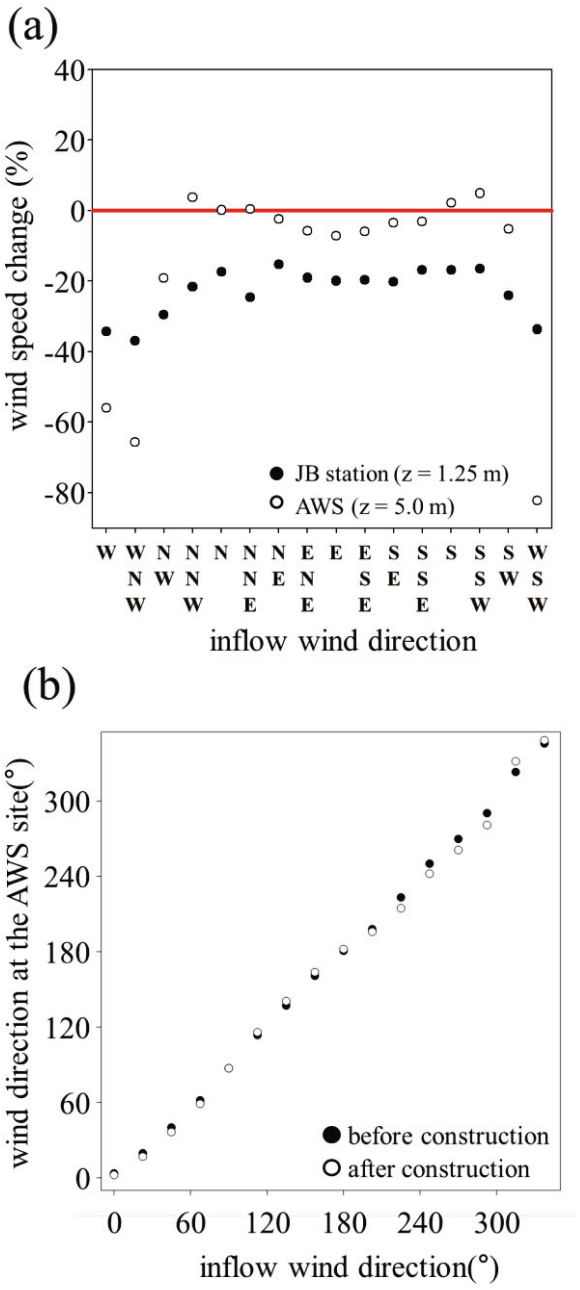

Fig. 5. (a) Percentage wind-speed changes simulated after the construction of JB station, at the AWS (z = 5 m) and at the station itself (z = 1.25 m) (rectangle in Fig. 1). (b) Comparison of wind directions at the AWS (z = 5 m) before and after construction of JB station. In (a), the percentage wind-speed changes at JB Station are averaged over the area indicated by the red rectangle in Fig. 1.

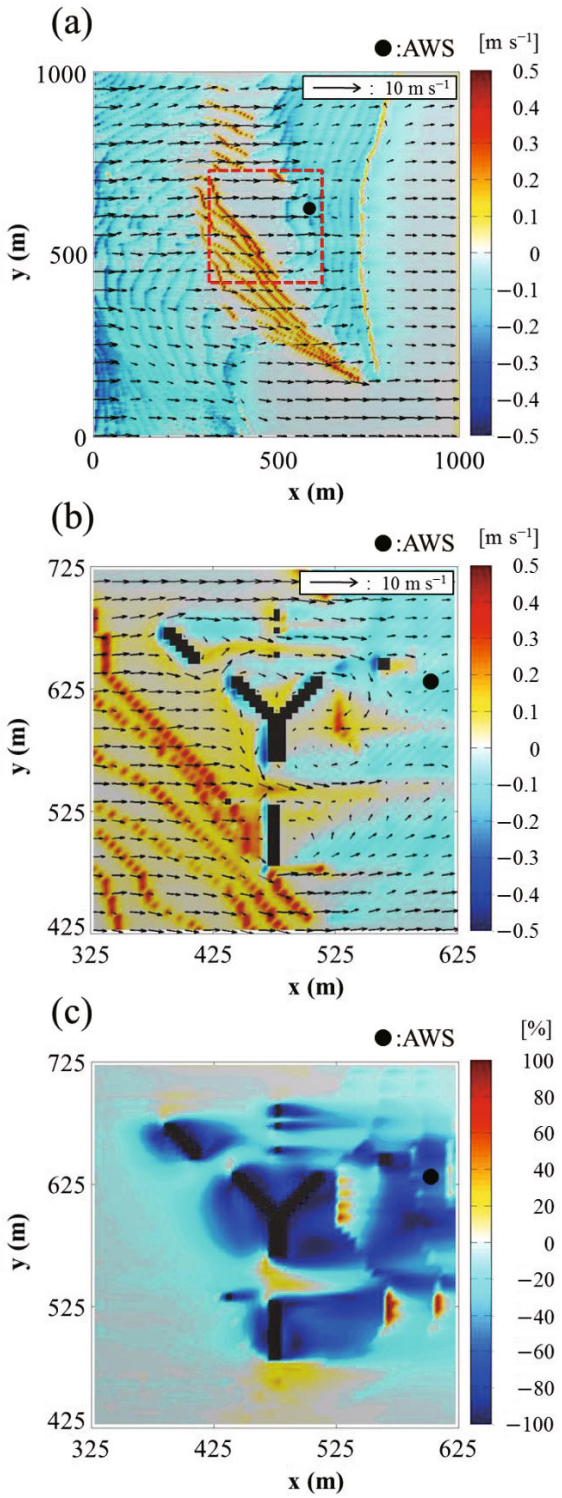

Fig. 6. Horizontal wind vectors and fields of the vertical wind component near the surface (z = 1.25 m) (a) before and (b) after the construction of JB Station, and (c) the difference in horizontal wind speed before and after the construction in the westerly case. The wind fields in (b) and (c) are taken from the area in the red-dashed rectangle in (a).

Wind speeds increased slightly after the construction of the station for five inflow directions: north-northwesterly (3.8%), northerly (0.4%), north-northeasterly (0.4%), southerly (2.1%), and south-southwesterly (5.0%). These increases initially occurred between the station buildings, due to channeling effects (Wang and Takle, 1996; Kim and Kim, 2009), which then enhanced the flows at the AWS. For the other inflow directions, the average surface wind speed around JB Station decreased by 22.9%. From the average wind speeds in the JB-before and JB-after cases, west-northwesterly (−36.9%) and westerly (−34.3%) winds showed particularly substantial reductions in wind speed. These reductions were less prominent for northeasterly (−15.3%) and southerly (−16.9%) winds (Fig. 5a). Wind direction was not notably affected (average change: 4.2°) (Fig. 5b).

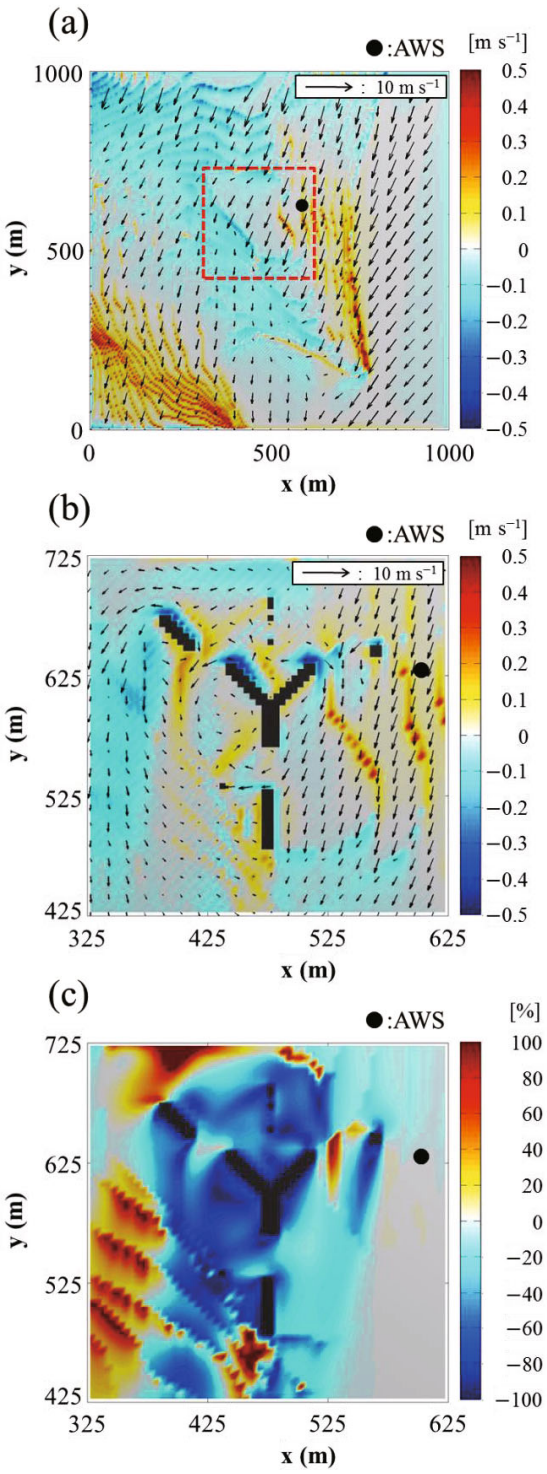

Fig. 7. As in Fig. 6 but for the north-northeasterly case.

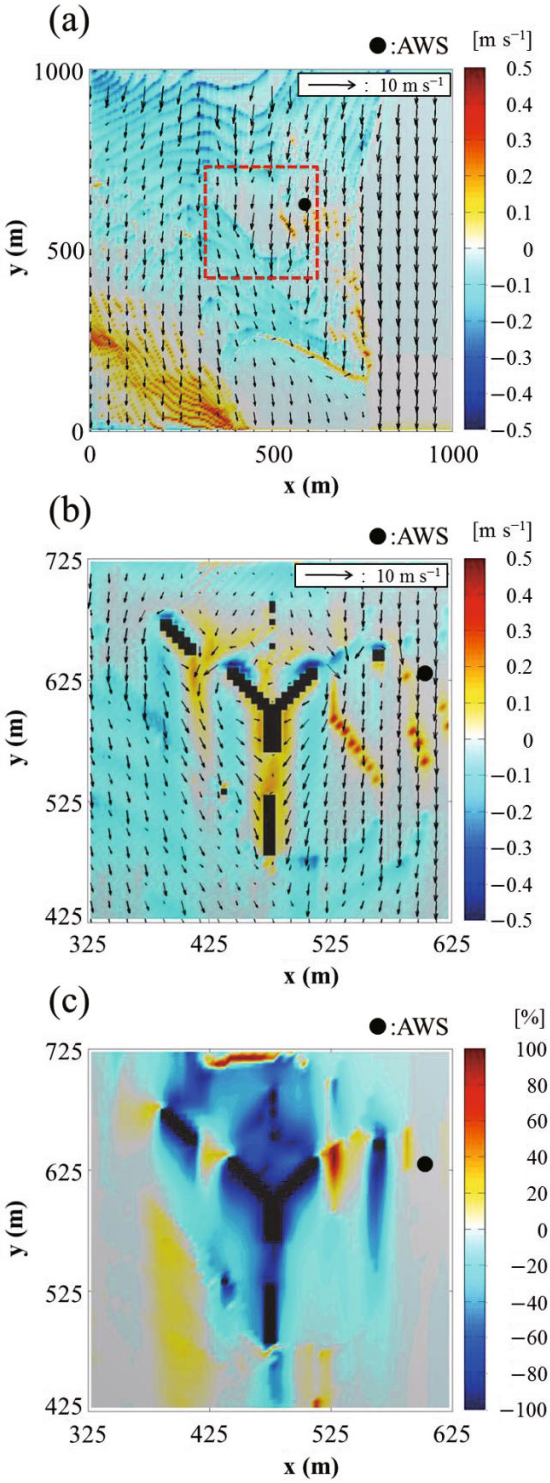

Fig. 8. As in Fig. 6 but for the northerly case.

3.2.2. *Westerly winds (270°)*

The terrain had many overall effects on westerly flows. In the valley located to the west of JB Station, air flowed down and up the west and east slopes of the valley, respectively, and downward flows appeared along the east slope of the valley (Fig. 6a). Flows around JB Station had horizontal wind speeds of 3.5 m s^{-1} to 4.0 m s^{-1}, and wind speed decreased to the east of JB Station along the coast, although wind speeds were restored farther off the coast. In the JB-after case, the flows around JB Station were more complex due to flow distortions caused by the buildings (Fig. 6b). In the JB-before case, westerly winds flowed to the AWS unobstructed. However, the AWS is located to the east of JB Station, and flows were diverted by the buildings in the JB-after case, which were simulated as changes in wind direction at the AWS (Figs. 6a and b). Moreover, variations in wind speed around JB Station appeared between the JB-before and JB-after cases. On the east side of the buildings, wind speed mainly decreased due to secondary circulations, such as a recirculation zone; however, wind speed between buildings increased slightly due to channeling effects (Fig. 6c). In the JB-after case, the average near-surface (z = 1.25 m) wind speed at JB Station decreased by 34.3% compared to the JB-before case, while wind speed at the AWS (z = 5.0 m) decreased by 53.3%. The sudden reduction in wind speed between the two cases indicates that the AWS is located within the recirculation zone.

3.2.3. *North-northeasterly winds (22.5°)*

At JB Station, air flows from the ocean are weakened rapidly upon reaching land due to friction, and air flows up the slope on the east side of JB Station. Meanwhile, air flows down the eastern slope and up the northwestern slope of the valley located to the west of JB Station (Fig. 7a). In the JB-after case, the north-northeasterly inflows were distorted by the presence of the buildings (Fig. 7b). In contrast to the westerly winds, much smaller changes occurred in north-northeasterly wind speed (0.02 m s^{-1}) and direction (2.8°) after the construction of the station, due to the upwind location of the AWS relative to the station. The average near-surface (z = 1.25 m) wind speed decreased by 24.6% compared with the JB-before case. However, wind speeds to the west of the station increased because the flows were blocked by the maintenance building and intercepted by flows from the northwest direction (Fig. 7c).

3.2.4. *Northerly winds (0°)*

Northerly winds were predominantly downward flows that formed along the downhill slope, although upward flows appeared occasionally along the uphill slope near the station. Flows weakened rapidly near the southern coastline by the station (Fig. 8a). In the JB-after case, the flows were northeasterly to the east of the station and northwesterly to the west of the station, which converged downwind of the buildings (Fig. 8b). Wind speeds increased slightly in between

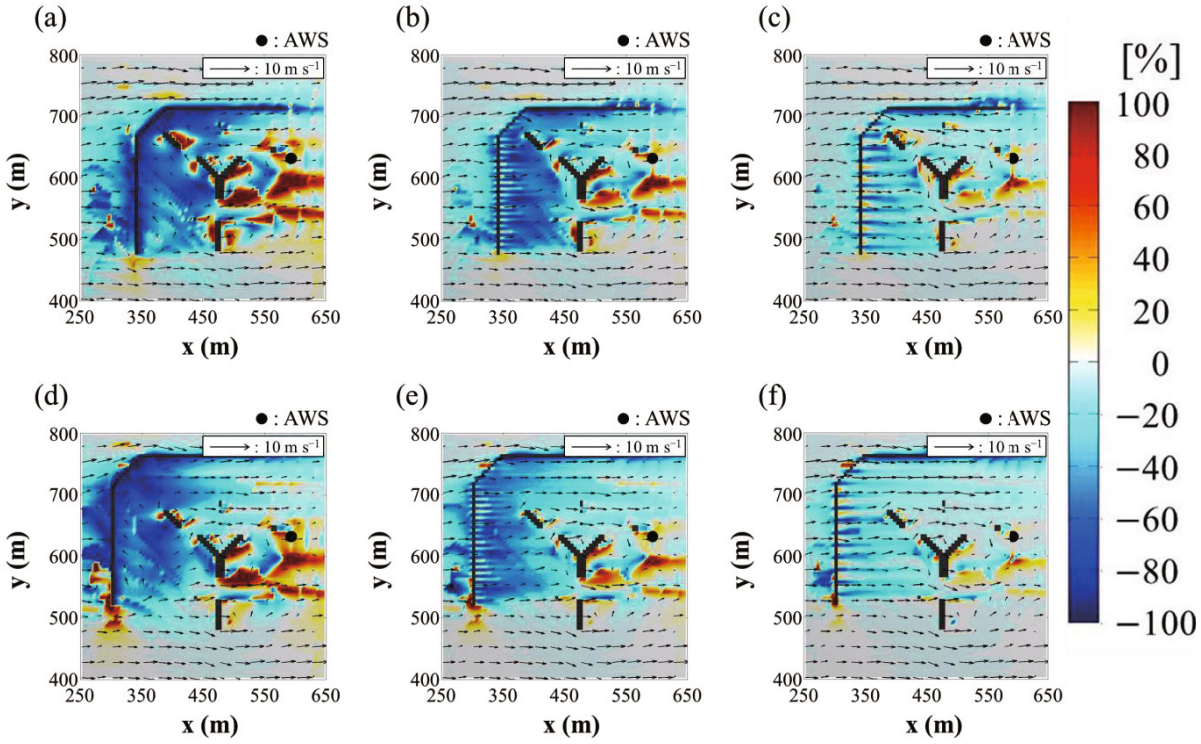

Fig. 9. Wind vectors and percentage changes in horizontal wind speed near the surface (z = 1.25 m) after the construction of the wind fences for different porosities and distances from JB station in the westerly case. The porosities of the wind fences are 0% [(a) and (d)], 50% [(b) and (e)], and 75% [(c) and (f)], and the distances from JB station are 2H [(a) to (c)] and 8H [(d) to (f)].

the upper-atmosphere observatory and the main building, as well as the maintenance and main buildings, due to channeling effects (Fig. 8c). The average near-surface (z = 1.25 m) wind speeds decreased by 17.3% compared with the JB-before case, while the wind speeds at the AWS (z = 5.0 m) increased by 0.4%. Moreover, wind speeds increased to the southwest of the main building compared with the JB-before case, as the northwesterly flows were blocked by the maintenance building.

3.2.5. *Effects of wind fences on the wind environment around JB Station*

Strong katabatic winds are relatively common at JB Station, and our analysis confirmed that the construction of the station has increased wind speeds in some directions around the station. Since wind is the biggest threat to the crews at this

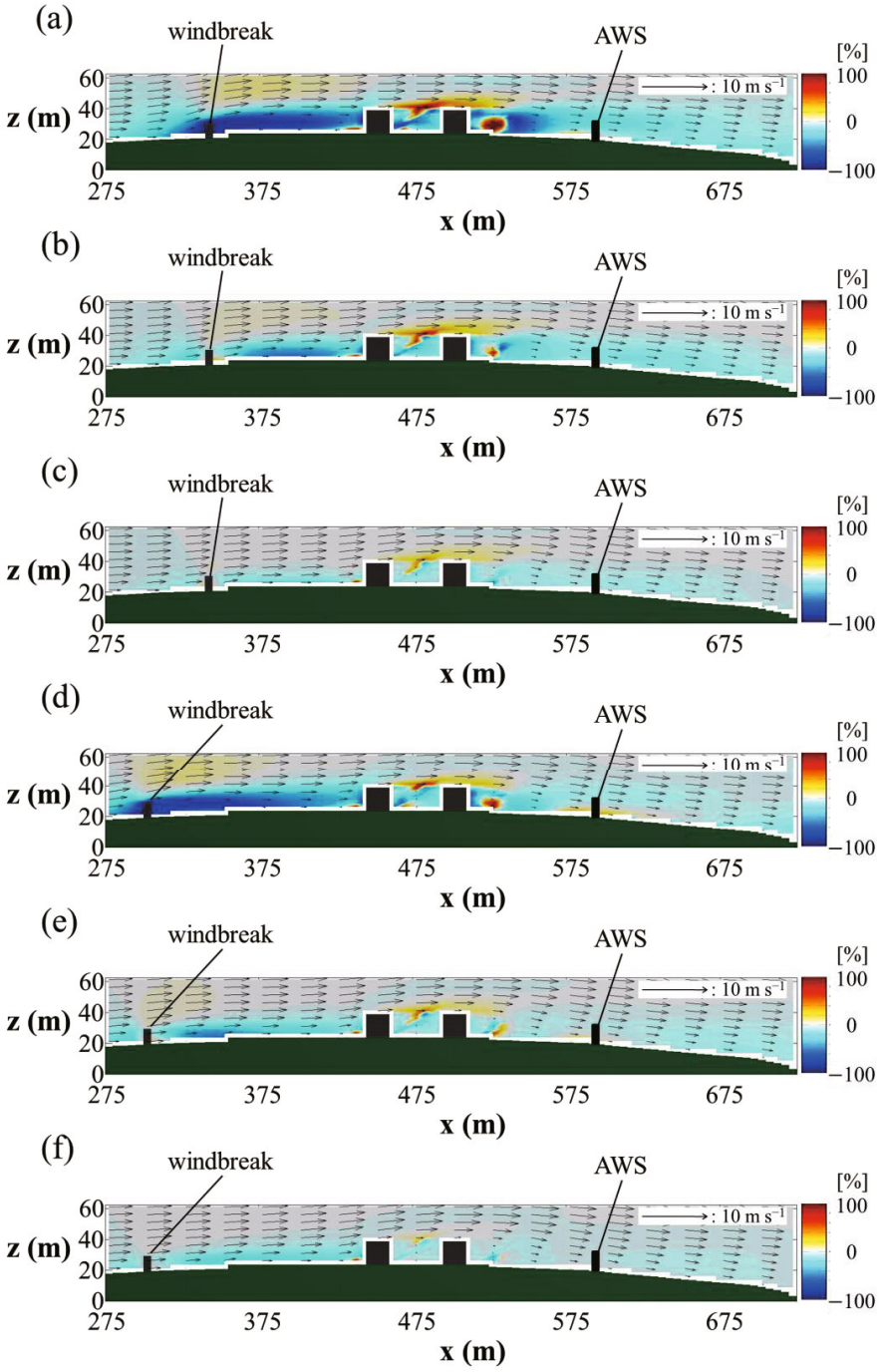

Fig. 10. Wind vectors and percentage changes in horizontal wind speed in the vertical plane of y = 622.5 m for different porosities and distances from JB station in the westerly case. The porosities of the wind fences are 0% [(a) and (d)], 50% [(b) and (e)], and 75% [(c) and (f)], and the distances from the JB station are 2H [(a) to (c)] and 8H [(d) to (f)].

Polar station, installation of wind fences may reduce damage to crews and facilities caused by strong winds. Therefore, we investigated the effects of wind fences with various construction parameters on wind speeds at JB Station and at the AWS. For the analysis, wind fences were positioned on the west and north sides of JB Station to target the strongest and most frequent westerly and northerly winds, based on AWS data analysis. We analyzed the effects of fence porosity (0%, 25%, 33%, 50%, 67% and 75%) and distance between the fences and JB Station (2H, 4H, 6H and 8H, where H is the height of the wind fences). Westerly winds were used as the inflow direction, as they are the most frequent and strongest winds at the station.

Figure 9 shows the surface wind vector field after the construction of the wind fences and the difference between the period after and before construction of the wind fences. Various wind-fence porosities (25%, 33%, 50%, 67% and 75%) were compared with the pre-wind-fence conditions, and the wind fences appeared to reduce wind speed without substantially changing wind direction (Figs. 9b, c, e and f). Lower wind-fence porosities were associated with larger reductions in wind speed in the area between the wind fences and the station, but increases in wind speed were simulated to the east of the station (Figs. 9 and 10). Reductions in wind speeds were significantly larger for the wind fences with a porosity of 0% than those with porosities of 25%, 33%, 50%, 67% and 75% in the windward direction of the fence compared with the conditions before the installation of the wind fence. However, this resulted in the formation of a recirculation area between the wind fences and the main building, which had a flow direction opposite to that of the inflow. In addition, the wind fence inhibited the increases in wind speeds observed in the JB-after case; however, strong winds occurred to the east of the station (Figs. 10a and d).

In the cases with distance to the station of 2H, wind fences with porosities of 0%, 25%, 33%, 50%, 67% and 75% decreased the average near-surface (z = 1.25 m) wind speeds by 15.3%, 17.6%, 17.4%, 16.0%, 10.6% and 7.7%, respectively. As the distance to the station became larger, the average near-surface wind speeds decreased (Fig. 11a). For the fixed distance to the station, the efficiency of wind fences for wind-speed reduction was maximized at porosities of 25% (2H) or 33% (4H–8H). Wind-speed changes at the AWS (z = 5.0 m) with distance and porosity showed a non-monotonic variation (Fig. 11b). The installation of wind fences with distance of 2H and porosities of 0%, 25%, 33%, 50%, 67% and 75%, decreased (changed) the wind speeds (directions) by 7.6% (3.5°), 5.8% (2.8°), 5.9% (3.1°), 8.5% (3.2°), 7.5% (2.6°) and 4.7% (2.2°), respectively (Fig. 11b). In the case of a distance of 4H, the wind-speed variation to porosities was similar to that in the cases of 2H. However, in the cases with distance of 8H, wind fences with porosities of 0%, 25%, 33% and 50% increased the wind speeds by about 6.9%, 7.1%, 4.4% and 1.9%, respectively; whereas, wind fences with porosities of 67% and 75% decreased the wind speed by about 2.3% and 1.5%, respectively. Wind direction at the AWS (z =5.0 m) was changed by about 1.3°, 0.5°, 0.7°, 1.0°, 1.2° and 0.9° by the installation of wind fences, with respective porosities of 0%, 25%, 33%, 50%, 67% and 75%. A previous study (Martin, 1995) reported that a reduction of wind speed by vertical wind fences on flat terrain was maximized for porosities of 40%–60%. However, in this study, the lower porosities (25%–33%), apart from the no-porosity cases, resulted in a larger decrease in wind speed around JB Station. This discrepancy was caused by the fact that wind fences were installed on a slightly inclined slope in this study. Analysis of the rates of change in near-surface wind speeds around JB Station showed that the maximum rates of change (increase or decrease) in wind speeds decreased monotonically as wind-fence porosity and distance to JB Station increased (Fig. 12).

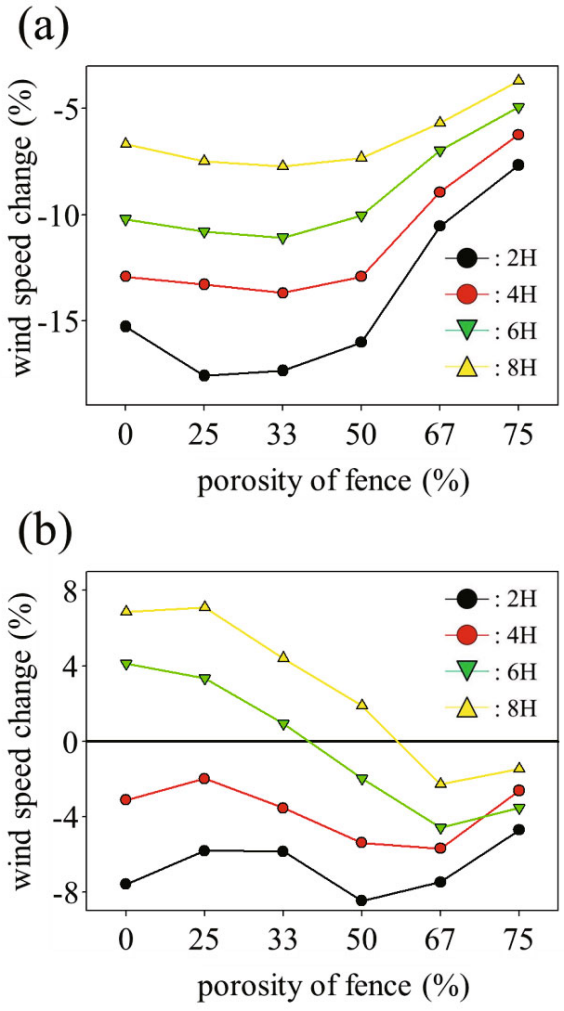

Fig. 11. Percentage changes in horizontal wind speed with wind-fence porosity and distance from JB station for (a) at the station itself (z = 1.25 m) and (b) at the AWS (z = 5.0 m).

4. Summary and conclusions

In this study, we analyzed the wind environment at JB Station in Terra Nova Bay, Antarctic, including the effects of

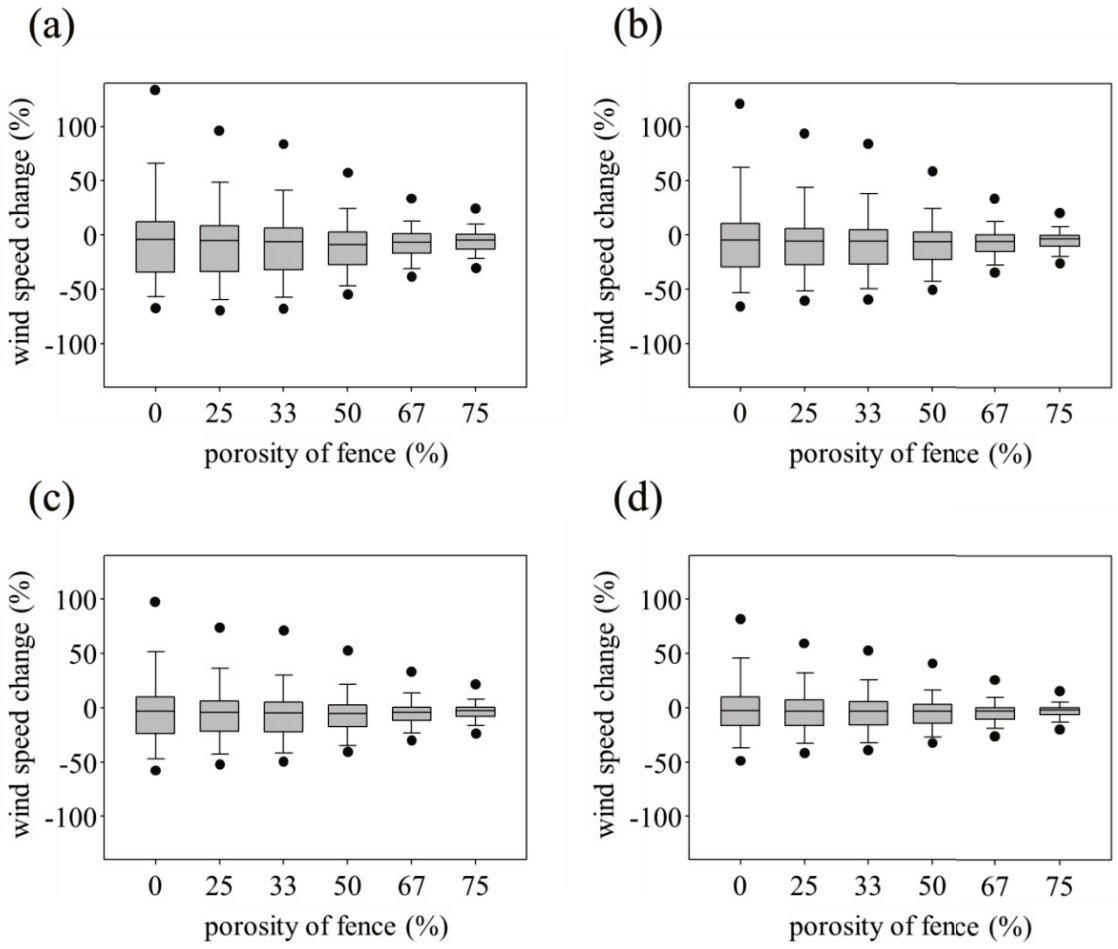

Fig. 12. Box plots for the percentage changes in near-surface (z = 1.25 m) wind speeds around JB Station in the cases with a distance to JB station of (a) 2H, (b) 4H, (c) 6H, and (d) 8H. The upper and lower black circles indicate the outliers; the bars above and below the boxes indicate the upper and lower extremes, respectively; and the upper, middle and lower segments of boxes indicate the upper quartiles, medians and lower quartiles, respectively.

the construction of JB Station on wind flow and AWS observations, and the effects of installing wind fences on wind behavior around JB Station. To investigate the effects of the construction of the station on wind at the AWS, we analyzed wind roses for the periods before (8 February 2010 to 31 October 2012) and after (1 January 2013 to 15 February 2015) construction of the station. To investigate the effects of JB Station on surface wind, numerical simulations were performed for 16 inflow directions (from northerly to north-northwesterly, at intervals of 22.5°) for both the JB-before and JB-after cases. In the after-JB case, changes in wind speed and wind direction were observed around JB Station and at the AWS. Westerly inflows along the mountain slopes had the highest wind speeds and occurrence frequencies, and the station had the greatest effects on westerly inflows, as the AWS is located to the east of JB Station. According to these results, the current location of the AWS near JB Station is unsuitable for research on katabatic winds. Moreover, if the AWS is transferred to the east or north side of JB Station, more accurate AWS data are expected due to smaller effects of the station.

Furthermore, we investigated the effects of installing wind fences on wind speed around JB Station. We assessed distances between the wind fences and the station of 2H, 4H, 6H and 8H, and wind fence porosities of 0%, 25%, 33%, 50%, 67% and 75%. Based on the results of the numerical simulation, reductions in near-surface (z = 1.25 m) wind speeds increased as the distance between the station and the wind fences decreased (except when porosity = 0%), and wind speed reduction was greatest at porosities of 25%–33%. However, wind fences with a porosity of 0% inhibited the increased flows around the buildings, but increased flows to the east of the station, which greatly affected winds at the AWS. Considering the numerical experiments from this study and results from previous studies, installing wind fences with porosities of 25%–33% would offer the best performance in promoting safety and reducing structural damage at JB Station.

Acknowledgements. The authors would like to thank the anonymous reviewers for their valuable comments and suggestions. This study was funded by a Korea Polar Research Institute project (PE16250). Hateak KWON is financially supported by PE17010 of Korea Polar Research Institute.

REFERENCES

Baik, J.-J., J.-J. Kim, and H. J. S. Fernando, 2003: A CFD model for simulating urban flow and dispersion. *J. Appl. Meteor.*, **42**, 1636–1648, doi: 10.1175/1520-0450(2003)042<1636:ACMFSU>2.0.CO;2.

Baik, J.-J., S.-B. Park, and J.-J. Kim, 2009: Urban flow and dispersion simulation using a CFD model coupled to a mesoscale model. *Journal of Applied Meteorology and Climatology*, **48**, 1667–1681, doi: 10.1175/2009JAMC2066.1.

Bromwich, D. H., 1989: An extraordinary katabatic wind regime at terra nova bay, Antarctica. *Mon. Wea. Rev.*, **117**, 688–695, doi: 10.1175/1520-0493(1989)117<0688:AEKWRA>2.0.CO;2.

Castro, I. P., and D. D. Apsley, 1997: Flow and dispersion over topography: A comparison between numerical and laboratory data for two-dimensional flows. *Atmos. Environ.*, **31**, 839–850, doi: 10.1016/S1352-2310(96)00248-8.

Cheng, J.-J., J.-Q. Lei, S.-Y. Li, and H.-F. Wang, 2016: Disturbance of the inclined inserting-type sand fence to wind-sand flow fields and its sand control characteristics. *Aeolian Research*, **21**, 139–150, doi: 10.1016/j.aeolia.2016.04.008.

Dong, Z. B., W. Y. Luo, G. Q. Qian, and H. T. Wang, 2007: A wind tunnel simulation of the mean velocity fields behind upright porous fences. *Agricultural and Forest Meteorology*, **146**, 82–93, doi: 10.1016/j.agrformet.2007.05.009.

Eichhorn, J., 2004: MISKAM-Handbuch zu Version 4 (with update for Version 6). Available online at http://www.lohmeyer.de/de/system/files/content/download/software/miskam_6_manual_english.pdf.

Gousseau, P., B. Blocken, T. Stathopoulos, and G. J. F. van Heijst, 2011: CFD simulation of near-field pollutant dispersion on a high-resolution grid: A case study by LES and RANS for a building group in downtown Montreal. *Atmos. Environ.*, **45**, 428–438, doi: 10.1016/j.atmosenv.2010.09.065.

Gowardhan, A. A., E. R. Pardyjak, I. Senocak, and M. J. Brown, 2011: A CFD-based wind solver for an urban fast response transport and dispersion model. *Environmental Fluid Mechanics*, **11**, 439–464, doi: 10.1007/s10652-011-9211-6.

Hertwig, D., G. C. Efthimiou, J. G. Bartzis, and B. Leitl, 2012: CFD-RANS model validation of turbulent flow in a semi-idealized urban canopy. *Journal of Wind Engineering and Industrial Aerodynamics*, **111**, 61–72, doi: 10.1016/j.jweia.2012.09.003.

Judd, M. J., M. R. Raupach, and J. J. Finnigan, 1996: A wind tunnel study of turbulent flow around single and multiple windbreaks, Part I: Velocity fields. *Bound.-Layer Meteor.*, **80**, 127–165, doi: 10.1007/BF00119015.

Kim, J.-J., 2007: The effects of obstacle aspect ratio on surrounding flows. *Atmosphere*, **17**, 381–391.

Kim, J.-J., and D.-Y. Kim, 2009: Effects of a building's density on flow in urban areas. *Adv. Atmos. Sci.*, **26**, 45–56, doi: 10.1007/s00376-009-0045-9.

Kim, J.-J., and J.-J. Baik, 2010: Effects of street-bottom and building-roof heating on flow in three-dimensional street canyons. *Adv. Atmos. Sci.*, **27**, 513–527, doi: 10.1007/s00376-009-9095-2.

Lee, S.-J., and H.-B. Kim, 1999: Laboratory measurements of velocity and turbulence field behind porous fences. *Journal of Wind Engineering and Industrial Aerodynamics*, **80**, 311–326, doi: 10.1016/S0167-6105(98)00193-7.

Ma, Y. M., 1992: Preliminary study on vertical velocity caused by katabatic wind in Antarctica and its influence on atmospheric circulation. *Adv. Atmos. Sci.*, **9**, 247–250, doi: 10.1007/BF02657515.

Martin, P., 1995: Wind protective fences of PARAWEB compositions. *Techtextil-Symposium* 1995, Lecture No. 537, 1–8.

Mitsuhashi, H., 1982: Measurements of snowdrifts and wind profiles around the huts at Syowa station in Antarctica. *Antarctic Record*, **75**, 37–56.

Nylen, T. H., A. G. Fountain, and P. T. Doran, 2004: Climatology of katabatic winds in the McMurdo dry valleys, southern Victoria Land, Antarctica. *J. Geophys. Res.*, **109**, doi: 10.1029/2003JD003937.

Stathopoulos, T., 2006: Pedestrian level winds and outdoor human comfort. *Journal of Wind Engineering and Industrial Aerodynamics*, **94**, 769–780, doi: 10.1016/j.jweia.2006.06.011.

Tominaga, Y., A. Mochida, T. Shirasawa, R. Yoshie, H. Kataoka, K. Harimoto, and T. Nozu, 2004: Cross comparisons of CFD results of wind environment at pedestrian level around a high-rise building and within a building complex. *Journal of Asian Architecture and Building Engineering*, **3**, 63–70, doi: 10.3130/jaabe.3.63.

Versteeg, H. K., and W. Malalasekera, 1995: *An Introduction to Computational Fluid Dynamics*: *The Finite Volume Method*. Longman, Malaysia, 257 pp.

Wang, H., and E. S. Takle, 1996: On shelter efficiency of shelterbelts in oblique wind. *Agricultural and Forest Meteorology*, **81**, 95–117, doi: 10.1016/0168-1923(95)02311-9.

Weber, N. J., M. A. Lazzara, L. K. Keller, and J. J. Cassano, 2016: The extreme wind events in the ross island region of Antarctica. *Wea. Forecasting*, **31**, 985–1000, doi: 10.1175/WAF-D-15-0125.1.

Yakhot, V., S. A. Orszag, S. Thangam, T. B. Gatski, and C. G. Speziale, 1992: Development of turbulence models for shear flows by a double expansion technique. *Physics of Fluids A*: *Fluid Dynamics*, **4**, 1510–1520, doi: 10.1063/1.858424.

You, K.-P., and Y.-M. Kim, 2009: Effect of protection against wind according to the variation porosity of wind fence. *Environmental Geology*, **56**, 1193–1203, doi: 10.1007/s00254-008-1219-y.

Yu, Y., X. M. Cai, and X. S. Qie, 2007: Influence of topography and large-scale forcing on the occurrence of katabatic flow jumps in Antarctica: Idealized simulations. *Adv. Atmos. Sci.*, **24**, 819–832, doi: 10.1007/s00376-007-0819-x.

Zhang, N., J.-H. Kang, and S.-J. Lee, 2010: Wind tunnel observation on the effect of a porous wind fence on shelter of saltating sand particles. *Geomorphology*, **120**, 224–232, doi: 10.1016/j.geomorph.2010.03.032.